

Article

Thermodynamic Modeling and Performance Analysis of a Combined Power Generation System Based on HT-PEMFC and ORC

Hyun Sung Kang^{1,2}, Myong-Hwan Kim³ and Yoon Hyuk Shin^{1,*}

¹ Eco-Friendly Vehicle R & D Division, Korea Automotive Technology Institute, 303 Pungse-Ro, Pungse-Myeon, Cheonan-Si 330-912, Korea; hskang@katech.re.kr

² Department of Mechanical Engineering, Korea University, 409 Innovation Hall Building, Anam-Dong, Sungbuk-Gu, Seoul 02841, Korea

³ Hydrogen Fuel Cell Mobility R&D Center, Korea Automotive Technology Institute, 303 Pungse-Ro, Pungse-Myeon, Cheonan-Si 330-912, Korea; kimmh@katech.re.kr

* Correspondence: yhshin@katech.re.kr; Tel.: +82-41-559-3284; Fax: +82-41-559-3235

Received: 12 October 2020; Accepted: 23 November 2020; Published: 24 November 2020



Abstract: Recently, the need for energy-saving and eco-friendly energy systems is increasing as problems such as rapid climate change and air pollution are getting more serious. While research on a power generation system using hydrogen energy-based fuel cells, which rarely generates harmful substances unlike fossil fuels, is being done, a power generation system that combines fuel cells and Organic Rankine Cycle (ORC) is being recognized. In the case of High Temperature Proton Exchange Membrane Fuel Cell (HT-PEMFC) with an operating temperature of approximately 150 to 200 °C, the importance of a thermal management system increases. It also produces the waste heat energy at a relatively high temperature, so it can be used as a heat source for ORC system. In order to achieve this outcome, waste heat must be used on a limited scale within a certain range of the temperature of the stack coolant. Therefore, it is necessary to utilize the waste heat of ORC system reflecting the stack thermal management and to establish and predict an appropriate operating range. By constructing an analytical model of a combined power generation system of HT-PEMFC and ORC systems, this study compares the stack load and power generation performance and efficiency of the system by operating temperature. In the integrated lumped thermal capacity model, the effects of stack operating temperature and current density, which are important factors affecting the performance change of HT-PEMFC and ORC combined cycle power generation, were compared according to operating conditions. In the comparison of the change in power and waste heat generation of the HT-PEMFC stack, it was shown that the rate of change in power and waste heat generation by the stack operating temperature was clearly changed according to the current density. In the case of the ORC system, changes in the thermal efficiency of the ORC system according to the operating temperature of the stack and the environmental temperature (cooling temperature) of the object to which this system is applied were characteristic. This study is expected to contribute to the establishment of an optimal operation strategy and efficient system configuration according to the subjects of the HT-PEMFC and ORC combined power generation system in the future.

Keywords: high temperature proton exchange membrane fuel cell; thermal management; organic rankine cycle; plate heat exchanger; waste heat recovery; cooling system; thermodynamic modeling

1. Introduction

Today, the need to expand power generation systems utilizing eco-friendly and waste heat energy to tackle climate changes is increasing, and active research on hydrogen fuel cell generation (electricity

generation) and a cogeneration system capable of utilizing waste heat is being done. Unlike engine or boiler-based power generation systems that generate power through a combustion process that uses fossil fuels to produce thermal energy and emission, hydrogen fuel cell systems is an eco-friendly power generator of electricity, thermal energy, and water through the chemical bonding process of hydrogen and oxygen.

The Solid Oxide Fuel cell (SOFC) based micro-cogenerative power system is being actively researched, and modeling research for predicting appropriate operating conditions is being considered for important research project purposes. Arpino et al. investigated the factors that influence the measurement uncertainty for combined heat and power design using SOFC [1]. In addition, they studied the correlation between the 0D model of those SOFC-based systems and the collected data. Additionally, an effective thermal management strategy through fuel utilization adjustments was presented for optimizing cogenerative power system operation [2]. Duhn et al. conducted an analytical study of the cooling plate design to improve operational efficiency by ensuring the pressure drop uniformity of the gas distributor of the SOFC system [3]. As described above, in a fuel cell-based power generation system having a high operating temperature, optimum control of the working fluid is important in addition to proper operating temperature and pressure drop formation in order to improve the efficiency and performance of the system.

In the case of High Temperature Proton Exchange Membrane Fuel Cell (HT-PEMFC), there is an advantage in that it can utilize waste heat at a relatively high temperature (150 °C or higher) with highly efficient power generation. In order to secure the power efficiency and reliability of such HT-PEMFC, a thermal management system is essential to maintain a high operating temperature [4,5]. As the operating temperature of the stack must be kept constant, the stack coolant must be used within a controlled temperature. Consequently, a thorough examination of the appropriate operating range of waste heat utilization (heat exchange) reflecting the respective stack thermal management and system control thereto, should be performed for the optimal design of cogeneration using HT-PEMFC and waste heat recovery [6,7].

Among the fuel cells, the PEMFC exhibits a relatively high power density and power efficiency, and it can minimize noise and residual emissions. It is divided into Low Temperature Proton Exchange Membrane Fuel Cell (LT-PEMFC) with an operating temperature of 60 to 80 °C and HT-PEMFC with an operating temperature of 100 °C or more. The power efficiency of HT-PEMFC appears to be approximately 45 to 60% [8]. Currently, research is being carried out on the cogeneration system suitable for each operation characteristic of each PEMFC type [9]. The advantage of HT-PEMFC is the simplification of the water management device configuration due to the high operating temperature as well as the generation of highly useful waste heat. Specifically, if the liquid cooling system is applied to HT-PEMFC thermal management with an operating temperature of 100 °C or higher, waste heat exchange with higher utilization is possible, which is advantageous for cogeneration and trigeneration systems [10]. Najafi et al. compared the performance and efficiency of the HT-PEMFC trigeneration system according to operation strategies during a certain operating period while the research team carried out a study on a trigeneration system to which both LT-PEMFC and HT-PEMFC were applied. Furthermore, research on warm-up strategies to quickly increase the stack operating temperature when the HT-PEMFC starts up was conducted [11]. Thus, based on the previous studies, it seems that the HT-PEMFC-based cooling and heating system can be selectively applied according to the operation strategy and subject.

It is important to secure the performance and efficiency of the waste heat recovery system in order to expand the subjects for application and functionality of the combined power generation system using such HT-PEMFC. This is one of the most important factors in selecting a target building and power system to secure electric energy with high utilization at a certain level depending on the operating environment [12,13]. Therefore, today, active research on Organic Rankine Cycle (ORC) system using stack waste heat energy in addition to fuel cell systems is being done [14]. Dickes' research team experimentally examined the temperature distribution of the working fluid for power

generation in the evaporator heat exchanger in the ORC power system, and Jang's research team conducted a study on the performance of the compact ORC system at the 1 kW-level using a heat source in the range of 100 to 140 °C [15,16]. In addition, Jeong's research team conducted a study on the heat exchange performance and characteristics of the plate heat exchanger for each working fluid operating condition applied to the ORC system [17]. S.C. Yang et al. conducted a pilot study on an ORC power generation system at the 3 kW-level, capable of utilizing waste heat at 100 °C [18]. In the case of HT-PEMFC, the inlet temperature and mass flow rate of the coolant must be kept relatively constant in order to secure appropriate power efficiency at a relatively high operating temperature [19]. This is a limiting factor that must be reflected in the operational design of waste heat utilization systems such as ORC power generation and is the reason for the need to optimize the integrated system linked to the stack thermal management system. To this end, it may be useful to introduce a HT-PEMFC and ORC power generation integrated system modeling, as well as a confirmation and verification process of power generation performance and efficiency range according to the application subject and operating conditions.

In this study, through an analytical method based on the existing HT-PEMFC and ORC power generation system model, the power generation performance and efficiency range according to the operating conditions of the HT-PEMFC and ORC combined power generation system considering stack thermal management were confirmed, and the rate of change of power generation performance (effect on power generation performance change) for each control factor for the combined power generation system was presented. For this, a system analysis was conducted to predict system performance and efficiency according to changes in operating conditions such as stack operating temperature, current density, and ORC cooling temperature for a combined power generation system composed of a lumped thermal capacity model.

2. System Description Based on HT-PEMFC and ORC

Figure 1 shows the model composition for performance prediction and comparative analysis of the combined system consisting of the HT-PEMFC subsystem for cooling of the HT-PEMFC and the ORC subsystem for waste heat recovery power generation. The HT-PEMFC subsystem and the ORC subsystem, each with a fluid flow diagram, share an evaporator. The coolant of the HT-PEMFC subsystem was selected as Tri-ethylene glycol (TEG) since its phase does not change at the operating temperature of HT-PEMFC, which is 423~463 K. It follows the black solid line in Figure 1. The HT-PEMFC subsystem consists of an auxiliary heater/cooler, thermal storage, 3-way valve, cooling pump, and evaporator heat exchanger. The auxiliary heater/cooler is configured to keep the inlet temperature of PEMFC constant regardless of the influence of the ORC subsystem when the thermal power of the HT-PEMFC and the heat supplied to the ORC is not the same during the initial system startup. The 3-way valve is configured to meet the same flow conditions as the thermal power of HT-PEMFC and the heat exchange amount of the ORC evaporator. The cooling pump was controlled so that it would meet the flow condition in which the temperature difference between the inlet and outlet of HT-PEMFC satisfies 5 K.

To simplify the analysis of this system, the study followed subsequent assumptions:

1. All equipment of the system follows the lumped model and ignores heat loss.
2. The pressure loss in the pipe through which the stack coolant and working fluid travel is ignored.
3. Temperature and cell voltage are evenly distributed over the entire electrode of HT-PEMFC, and the reaction gas mixture is an ideal gas fluid.
4. The cathode charge transfer coefficient and the anode charge transfer coefficient are the same.
5. The isentropic efficiency of the expander is 60%, and the overall efficiency of the refrigerant pump is 50%.
6. In the condenser of the ORC system, the working fluid is sufficiently subcooled, and the existing superheat of the evaporator is 5 K.

7. The pressure loss of the evaporator reflected only the pressure loss on the heat source side, and only the loss due to friction was considered.

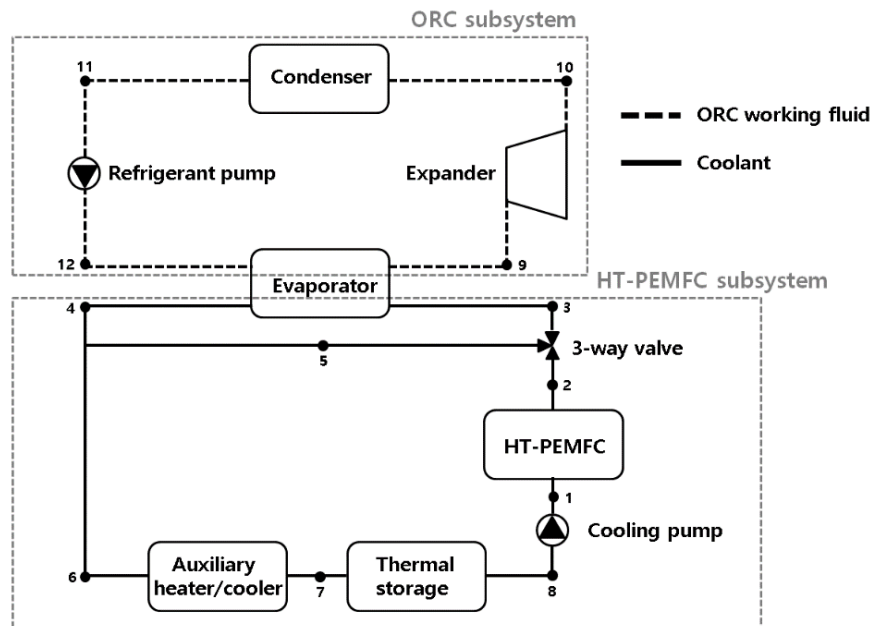
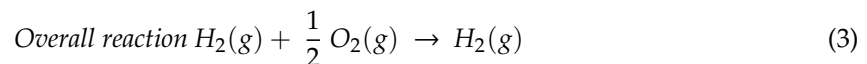
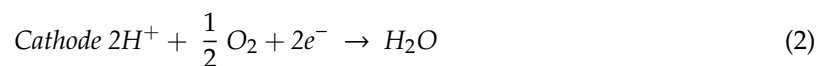


Figure 1. Schematic diagram of combined system.

3. Combined HT-PEMFC and ORC System Modeling

3.1. Thermodynamic Model of HT-PEMFC

The HT-PEMFC model applied in this analysis can be used by setting the operating temperature range of 120 to 200 °C, the cathode stoichiometric ratio range of 2 to 5, and the CO concentration range of 0.1 to 10%. Using a previously studied model as a reference [20,21], it is a one-dimensional isothermal model, HT-PEMFC based on PBI, and the electrochemical reaction in the fuel cell is as follows [22]:



The overall cell voltage of the stack is calculated through the overpotential loss acting on the cathode and the overpotential loss acting on the anode at the ideal standard potential as shown in the Equation (4). The overpotential is divided into the activation overpotential (η_{act}), ohmic overpotential (η_{ohmic}), and concentration overpotential (η_{conc}) [23]. The activation overpotential is affected by the Tafel equation and the charge transfer coefficient while the ohmic overpotential is affected by the thickness of the membrane and the catalyst. The last term, concentration overpotential, represents the effect of cathode stoichiometry.

The ideal standard potential (V_{ideal}) is calculated by the variation of Gibbs free energy (Δgf) through electrochemical reaction and Faraday Constant (F) as shown in Equations (5) and (6), but in this model, the open circuit voltage of a reference [20] is used.

$$V_{cell} = V_{ocv} - \eta_{act} - \eta_{ohmic} - \eta_{conc} \quad (4)$$

$$\Delta gf = gf_{H_2O} - gf_{H_2} - gf_{O_2} \quad (5)$$

$$V_{ideal} = -\frac{\Delta gf}{2F} \quad (6)$$

Activation overpotential acting on cathode and anode is obtained from the following equations:

$$\eta_{act} = \frac{RT_{cell}}{4\alpha_c F} \ln\left(\frac{I + I_0}{I_0}\right) + \frac{RT_{cell}}{\alpha_a F} \sinh^{-1}\left(\frac{I}{2k_{eh}\theta_{h2}}\right) \quad (7)$$

$$\alpha_c = a_0 T_{cell} + b_0 \quad (8)$$

$$I_0 = a_1 e^{-b_1 T_{cell}} \quad (9)$$

where R is the universal gas constant, T_{cell} is the operating temperature, α_c is the cathode charge transfer coefficient, F is the faraday constant, I is the current density, k_{eh} is the hydrogen electro-oxidation rate constant, θ_{h2} is the hydrogen surface coverage, I_0 is the exchange current density, λ_{air} is the cathode stoichiometry ratio, and α_a is the anode charge transfer coefficient, and it is assumed to be the same as the cathode charge transfer coefficient.

Ohmic overpotential and concentration overpotential acting on the cathode is given by:

$$\eta_{ohmic} = R_{ohmic} I \quad (10)$$

$$R_{ohmic} = a_2 T_{cell} + b_2 \quad (11)$$

$$\eta_{conc} = \frac{R_{conc}}{\lambda_{air} - 1} I \quad (12)$$

$$R_{conc} = a_3 T_{cell} + b_3 \quad (13)$$

Linear regression was used for the cathode charge transfer coefficient, ohmic resistance (R_{ohmic}), and concentration resistance (R_{conc}), and the exchange current density was expressed as an exponential function type. The values of the regressions used are shown in Table 1.

Table 1. Numerical value for regressions used in the High Temperature Proton Exchange Membrane Fuel Cell (HT-PEMFC) model.

Parameters	Values	Unit
Charge transfer constant, a_0	2.761×10^{-3}	[K ⁻¹]
Charge transfer constant, b_0	-0.9453	-
Limiting current constant, a_1	3.3×10^3	[A]
Limiting current constant, b_1	-0.04368	-
Ohmic loss constant, a_2	-1.667×10^{-4}	[Ω/K]
Ohmic loss constant, b_2	0.2289	[Ω]
Diffusion limitation constant, a_3	-8.203×10^{-4}	[Ω/K]
Diffusion limitation constant, b_3	0.4306	[Ω]

It was assumed that all cell unit performances of the HT-PEMFC were the same, and the electric power (W_{FC}) and thermal power (Q_{FC}) of HT-PEMFC were calculated in proportion to the number of cells (N_{cell}) and single cell active area (A_{cell}) as in Equations (14) and (15). Moreover, the power efficiency (η_{FC}) of HT-PEMFC can be obtained as in Equation (16) based on the lower heating value (LHV) of hydrogen. Table 2 shows the parameters used in the HT-PEMFC model

$$W_{FC} = N_{cell} V_{cell} I A_{cell} \quad (14)$$

$$Q_{FC} = N_{cell} \left(\frac{LHV}{2F} - V_{cell} \right) I A_{cell} \quad (15)$$

$$\eta_{FC} = \frac{W_{FC}}{N_{cell} \frac{LHV}{2F} I A_{cell}} \quad (16)$$

Table 2. Operating parameters and empirical parameters used in the HT-PEMFC model.

Parameters	Values	Unit
Open circuit Voltage, V_{ocv}	0.95	[V]
Number of cells, N_{cell}	880	-
Single cell active area, A_{cell}	300	[cm ²]
Operating temperature, T_{cell}	433	[K]
Current density, I	0.4	[A/cm ²]
Universal gas constant, R	8.314	[J/mol·K]
Faraday constant, F	96485.3	[C/mol]
Cathode stoichiometry ratio, λ_{air} [24]	3	-
Hydrogen electro-oxidation rate constant, k_{eh} [24]	1.63818	[A/cm ²]
Hydrogen surface coverage, θ_{h2} [24]	0.14212	-
Low heating Value of hydrogen, LHV	239.92	[kJ/mol]

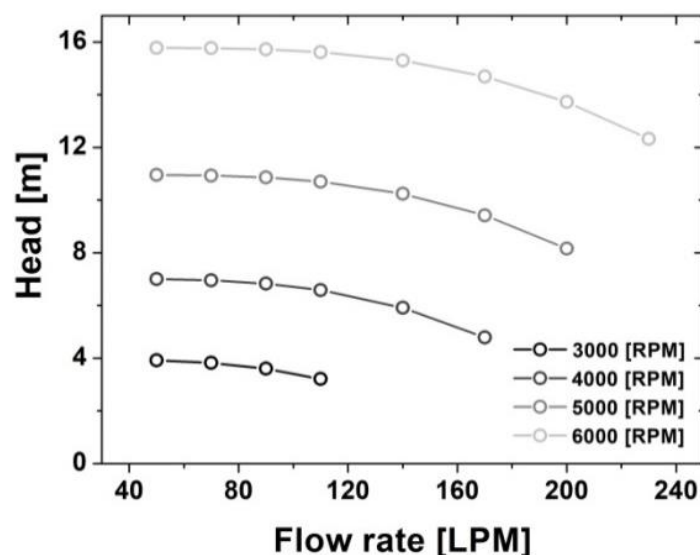
The thermal power generated by the HT-PEMFC was assumed to be heat-exchanged with the coolant by the Dittus-Boelter Equation (17), and the heat generated by auxiliary devices such as the cooling pump was ignored.

$$Nu = 0.023Re^{0.8}Pr^{0.4} \quad (17)$$

Furthermore, the pressure drop on the coolant side of the HT-PEMFC was reflected by the curve fitting the pressure drop according to the flow rate based on the experimental value. In general, the pressure drop on the coolant side of the stack is dependent on the flow path design of the cooling plate, and in this study, the pressure drop test value of the most widely commercialized vehicle stack with a level similar to the reaction area was applied to the model.

$$\Delta P_{FC} = 4074 + 1.86 \times 10^6 Q_{FC} + 3.184 \times 10^9 Q_{FC}^2 \quad (18)$$

As a cooling pump model used to transport Triethylene glycol (TEG), which is a stack coolant, a commercial pump for cooling of a maximum 100 kW stack that has a performance curve as shown in Figure 2 was applied [25].

**Figure 2.** The performance curve of the cooling pump.

3.2. Thermodynamic Model of ORC

Figure 3 shows the T-s diagram of the ideal ORC cycle and conceptually shows each state and system. In Figure 3, the movement from point 12 to point 9 refers to the section in which the liquid

working fluid changes to the gaseous state through the evaporator and is the section to recover waste heat from HT-PEMFC in the combined system. The vaporized working fluid generates power through the expander, which is the travel section from point 9 to 10, reducing the pressure. The working fluid with reduced pressure and temperature is liquefied in the travel section from point 10 to 11 through the condenser and maintains the pressure difference while transporting the liquefied working fluid through the pump.

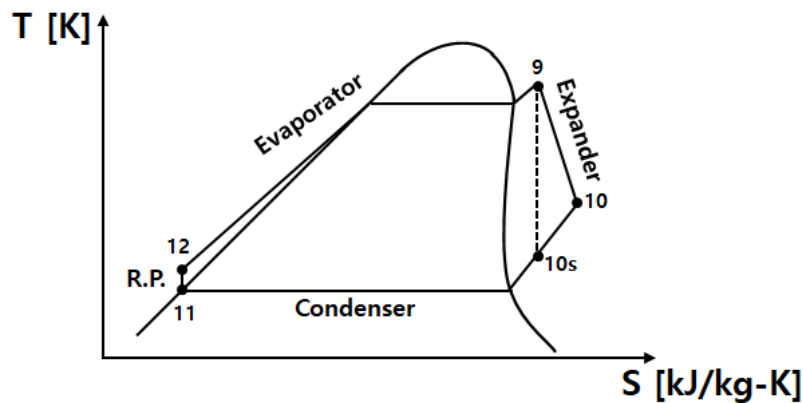


Figure 3. Thermodynamic T-s diagram for ideal Organic Rankine Cycle (ORC) cycle (R.P. is the meaning of refrigerant pump).

R245fa was selected as the working fluid used in this study considering the operating temperature range of the HT-PEMFC. The pressure on the evaporator side of the ORC power generation of the combined power generation system was set to 12 bar, and by setting the temperature range at the outlet side of the condenser to 293~308 K, the saturation pressure appropriate for the respective temperature was used.

All waste heat generated from the HT-PEMFC is heat-exchanged through the evaporator and is calculated as shown in Equation (19). \dot{Q}_{eva} is the amount of heat exchange of the evaporator, and \dot{m}_{ORC} is the mass flow rate of the working fluid of the ORC system. h means the enthalpy according to the temperature and pressure for each location indicated by each number on the T-s diagram.

$$\dot{Q}_{eva} = \dot{m}_{ORC}(h_9 - h_{12}) \quad (19)$$

The amount of power generated through the expander is W_{exp} and is calculated as in the Equation (20).

$$W_{exp} = \dot{m}_{ORC}(h_9 - h_{10}) \quad (20)$$

The amount of heat dissipated through the condenser is \dot{Q}_{con} and is calculated as in the Equation (21).

$$\dot{Q}_{con} = \dot{m}_{ORC}(h_{10} - h_{11}) \quad (21)$$

The power consumption of the refrigerant pump is W_{rp} and is calculated as in the Equation (22), taking into account the overall efficiency η_{rp} .

$$W_{rp} = \frac{\dot{m}_{ORC}(h_{12} - h_{11})}{\eta_{rp}} \quad (22)$$

The net power generated through the ORC system is calculated by the power generated by the expander and the power consumed by the refrigerant pump as shown in the Equation (23).

$$W_{ORC} = W_{exp} - W_{rp} \quad (23)$$

The thermal efficiency of the ORC system is η_{ORC} and is calculated by the net power of the ORC and the endothermic reaction through the evaporator as in the Equation (24).

$$\eta_{ORC} = \frac{W_{ORC}}{\dot{Q}_{eva}} \quad (24)$$

3.3. Analytical Model of the Evaporator Heat Exchanger

A heat exchanger model for the evaporator was constructed to calculate the mass flow rate required by the heat source according to the mass flow rate of the working fluid of the ORC power generation system and the inlet temperature of the heat source (stack coolant) side. The plate heat exchanger used in the experiment in Jeong's study was used as a reference for the shape information of the respective evaporator and is shown in Table 3. [17]. The basic geometric characteristics of the chevron plate heat exchanger are shown in Figure 4.

Table 3. Operating parameters of the chevron plate heat exchanger.

Parameters	Values	Unit
Effective width of plate, L_h	0.111	[m]
Vertical distance between ports, L_v	0.466	[m]
Plate thickness, t	0.0004	[m]
Chevron configuration pitch, λ_p	0.007	[m]
Plate channel gap, g	0.002	[m]
Flow channel hydraulic diameter, D_h	0.003389	[m]
Effective heat transfer area, A_{hx}	0.06105	[m ²]
Plate chevron angle, β	35	[°]
Plate thermal conductivity, k	15	[w/m-K]
Surface enlargement factor, φ	1.18	-
Working fluid channel number, N_{wf}	21	-
Heat source channel number, N_{hs}	22	-

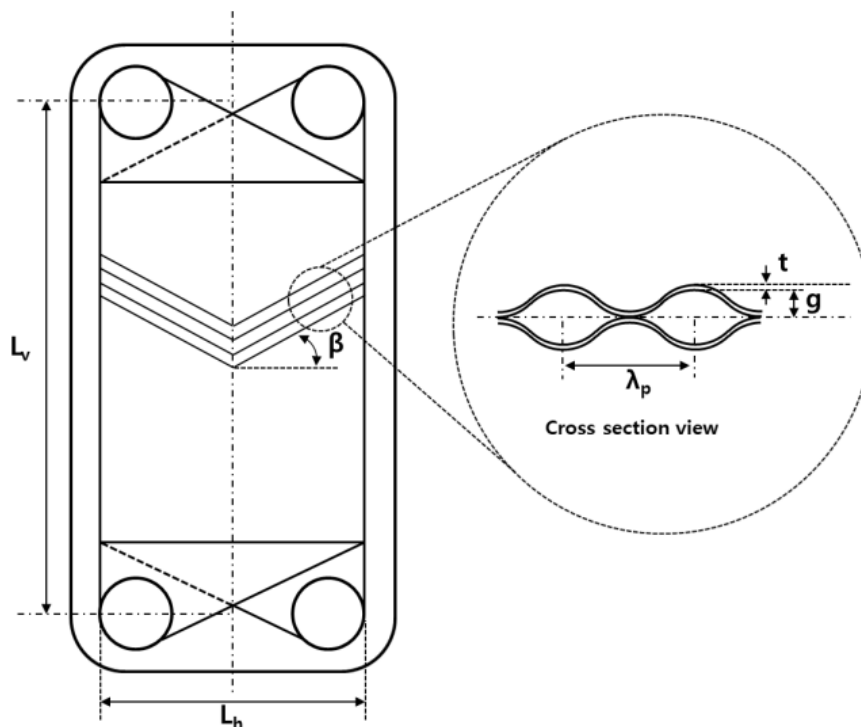


Figure 4. Basic geometric characteristics of chevron plate heat exchanger.

The overall heat transfer coefficient (U) of the Evaporator Heat Exchanger is calculated by the convective heat transfer coefficient of the working fluid (h_{wf}), the convective heat transfer coefficient of the heat source (h_{hs}), and the conduction heat transfer coefficient of the heat exchanger (k_p) as shown in the Equation (25).

$$\frac{1}{U} = \frac{1}{h_{wf}} + \frac{t}{k_p} + \frac{1}{h_{hs}} \quad (25)$$

The heat source is in a single-phase state in all operating areas, and the convective heat transfer coefficient in the single-phase state followed the Muley and Manglik correlation. Based on the Reynolds number, it followed the Equation (26) at 400 or below and followed the Equation (27) at 800 or more [26]. Moreover, the Nusselt number was interpolated using the transitional algorithm in the transition zone. Re_L is the Reynolds number in the liquid state, whereas Pr_L is the Prantle number in the liquid state. In addition, k_L is the heat transfer coefficient in the liquid state, while D_h is the hydraulic diameter of the plate heat exchanger.

$$h_{hs} = 0.44 \left(\frac{\beta}{30} \right)^{0.38} Re_L^{0.5} Pr_L^{0.33} \left(\frac{k_L}{D_h} \right) \quad (26)$$

$$D_0 = 0.2688 - 0.006967\beta + 7.244 \times 10^{-5}\beta^2$$

$$D_1 = 20.78 - 50.94\varphi + 41.1\varphi^2 - 10.51\varphi^3$$

$$D_2 = 0.728 + 0.0543 \sin\left(\frac{\pi\beta}{45} + 3.7\right)$$

$$h_{hs} = D_0 D_1 Re_L^{D_2} Pr_L^{0.33} \left(\frac{k_L}{D_h} \right) \quad (27)$$

The convective heat transfer coefficient in the two phase region of the evaporator's working fluid follows the Yan and Lin correlation and is as shown in Equation (28) [27]. Re_{eq} is the equivalent Reynolds number, Bo is the boiling number, G_{eq} is the equivalent mass flux. G is the channel mass flux. q is the heat flux. x is the vapor quality. μ_L is the dynamic viscosity of the liquid. ρ_L is the density of the liquid, and ρ_v is the density of the vapor.

$$h_{wf} = 1.926 Re_{eq}^{0.5} Pr_L^{0.33} Bo^{0.3} \left[1 - x + x \left(\frac{\rho_L}{\rho_v} \right)^{0.5} \right] \left(\frac{k_L}{D_h} \right) \quad (28)$$

$$Bo = \frac{q}{GA_{hx}} Bo = \frac{q}{GA_{hx}} \quad (29)$$

$$G_{eq} = G \left[1 - x + x \left(\frac{\rho_L}{\rho_v} \right)^{0.5} \right] \quad (30)$$

$$Re_{eq} = \frac{G_{eq} D_h}{\mu_L} \quad (31)$$

To compare and verify the analysis results based on the evaporator heat exchanger model constructed as described above and the previous experimental results, The validation analysis was conducted using the same conditions as in Jeong's study using R245fa as the working fluid and water as the heat source. As shown in Figure 5, the difference between Jeong's heat exchanger performance data that was previously studied and the analysis results in this study were within 3% approximately, and the analysis model constructed accordingly was confirmed to have a certain level of reliability.

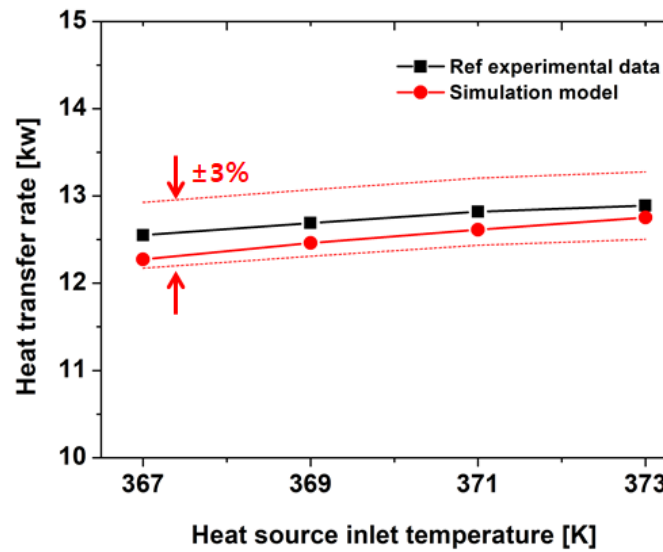


Figure 5. Validation of heat exchanger performance.

The pressure loss on the heat source side of the evaporator heat exchanger is ΔP_{eva} and is defined as the Equation (32) considering only the loss due to friction.

$$\Delta P_{eva} = f_{hs} \frac{L_v N_{hs} G^2}{2D_h \rho L} \quad (32)$$

f_{hs} follows the Darcy friction factor and is expressed as in the Equation (33) [17].

$$f_{hs} = 72.5 Re_L^{-0.045} \quad (33)$$

3.4. Performance of the Combined System (HT-PEMFC and ORC)

The total electric power produced by the combined system consisting of the HT-PEMFC and ORC is expressed as the sum of the power generated by the HT-PEMFC (W_{FC}), the power consumed by the cooling pump for the HT-PEMFC (W_{cp}), the power generated through ORC (W_{exp}), and the power consumed by the refrigerant pump (W_{rp}) as shown in the Equation (34).

$$W_{total} = W_{FC} - W_{cp} + W_{exp} - W_{rp} \quad (34)$$

In addition, the power efficiency of the combined system is expressed as the ratio of the total power of the combined system according to the LHV of HT-PEMFC, as shown in the Equation (35).

$$\eta_{system} = \frac{W_{total}}{N_{cell} \frac{LHV}{2F} IA_{cell}} \quad (35)$$

The whole system is analyzed using the commercial program Flomaster based on the law of conservation of energy (36), the law of conservation of mass (37), and the law of conservation of species (38).

$$\sum (\dot{m}h)_{in} + \sum \dot{Q}_{in} = \sum (\dot{m}h)_{out} + \sum \dot{Q}_{out} \quad (36)$$

$$\sum (\dot{m})_{in} = \sum (\dot{m})_{out} \quad (37)$$

$$\sum (\dot{m}x)_{in} = \sum (\dot{m}x)_{out} \quad (38)$$

4. Results and Discussion

4.1. Effect of Stack Temperature

In order to check the performance change according to the operating temperature and current density of the stack, the performance curves for each operating temperature (433 K, 443 K, 453 K, 463 K) and current density (0~0.5 A/cm²) were verified. As shown in Figure 6a, as the temperature increased, the stack's single cell voltage and efficiency increased as well because of the decrease in the cell activation overpotential. In addition, it tended to decrease when the current density increased. Furthermore, the stack electric power and thermal power showed a tendency to increase as the current density increased, but the percentage of increase in the electric power decreased although the percentage of increase in the thermal power increased. As the temperature of the stack increased, the stack electric power increased thanks to the increase in power efficiency, whereas the stack thermal power decreased. When the current density was 0.1 A/cm² and 0.4 A/cm² at a stack temperature of 433 K, the single cell voltage was 0.66 V and 0.47 V, the stack power efficiency was 53.7% and 38.1%, the stack electric power was 17.6 kW and 50 kW, and the stack thermal power was 15.2 kW and 81.3 kW.

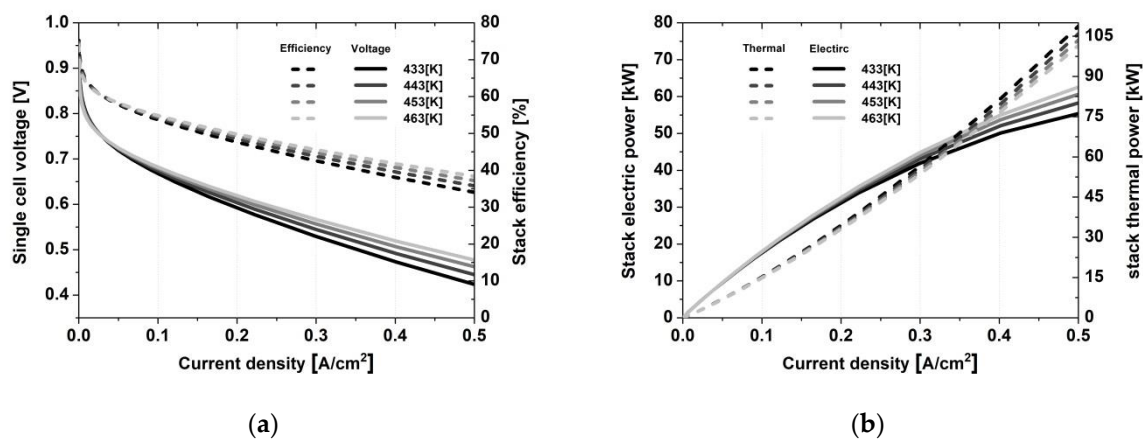


Figure 6. HT-PEMFC performance curve according to stack temperature and current density. (a) Single cell voltage and stack power efficiency; (b) Stack electric power and thermal power.

4.2. Effect of Working Fluid Mass Flow Rate in the ORC System

The performance change was analyzed by applying the evaporator model configured to calculate the performance according to the mass flow rate of R245fa, the working fluid of the ORC system, and the heat exchange amount of the evaporator. The evaporator pressure was selected as 12 bar considering the temperature level of the waste heat of the stack, and the condenser pressure was selected as 2.2 bar considering the extreme summer outdoor temperature. Moreover, the flow rate of the heat source (stack coolant, TEG) in which the superheat of the evaporator satisfies 5 K was calculated according to the corresponding inlet temperatures of 428 K, 448 K, and 468 K.

As shown in Figure 7a, as the mass flow rate of R245fa increased, the ORC net power increased linearly by the power consumption of the expander and the power consumption of the refrigerant pump. Although there was a change in performance according to the mass flow rate of the working fluid, the efficiency of the ORC system was relatively constant at about 7.69%, because all the conditions satisfied 5 K of superheat. In addition, as shown in Figure 7c, since the mass flow rate of the heat source (TEG) side where the superheat of the evaporator satisfies 5 K required a higher heat transfer coefficient as the inlet temperature of the heat source decreased, the mass flow rate increased. For the R245fa mass flow rate of 0.3 kg/s, the TEG-required mass flow rate was a maximum of 0.83 kg/s.

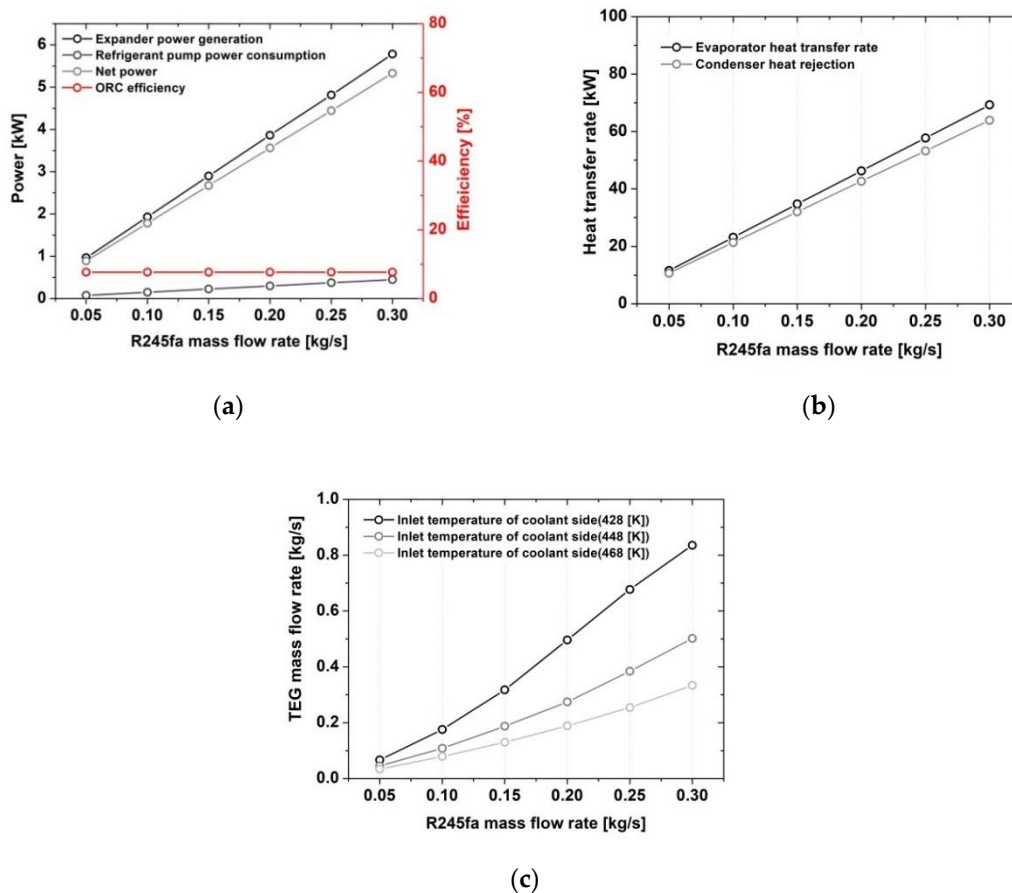


Figure 7. ORC system performance curve according to R245fa mass flow rate. (a) Electric power; (b) Evaporator and condenser heat transfer rate; (c) Mass flow rate of Tri-ethylene glycol (TEG) that satisfies superheat 5 K in the evaporator.

4.3. Effect of Stack Inlet Temperature in the Combined System

In order to analyze the combined system that merged the HT-PEMFC subsystem and the ORC subsystem, the transport pump controlled the mass flow rate so that the temperature difference at the inlet and outlet of the stack was 5 K. The mass flow rate was controlled through a 3-way valve so that all thermal power generated from the stack was exchanged with the evaporator of the ORC subsystem. The system performance was compared and analyzed after the inlet temperature conditions of the stack were selected as 433 K, 443 K, 453 K, and 463 K, and the current densities of the stack were 0.15 A/cm², 0.2 A/cm², 0.25 A/cm², 0.3 A/cm², 0.35 A/cm² and 0.4 A/cm².

As shown in Figure 8a, the mass flow rate of the cooling pump that satisfies the temperature difference between the inlet and outlet of the stack as 5 K is proportional to the current density. As the thermal power of the stack increased as shown in Figure 9d, the required convective heat transfer coefficient also increased, resulting in an increase in the mass flow rate that satisfied the operating conditions. As the inlet temperature of the stack increased, the physical properties of TEG changed, which influenced the formation of the mass flow rate of the cooling pump. The mass flow rate at the evaporator heat source (TEG) side of the ORC subsystem increased as the current density increased, but it decreased as the inlet temperature of the stack increased. The results of the mass flow rate of the cooling pump and the mass flow rate of the evaporator's heat source (TEG) according to the operating conditions, as well as the pressure drop of the stack and the pressure drop of the evaporator are shown in Figure 8c,d, respectively.

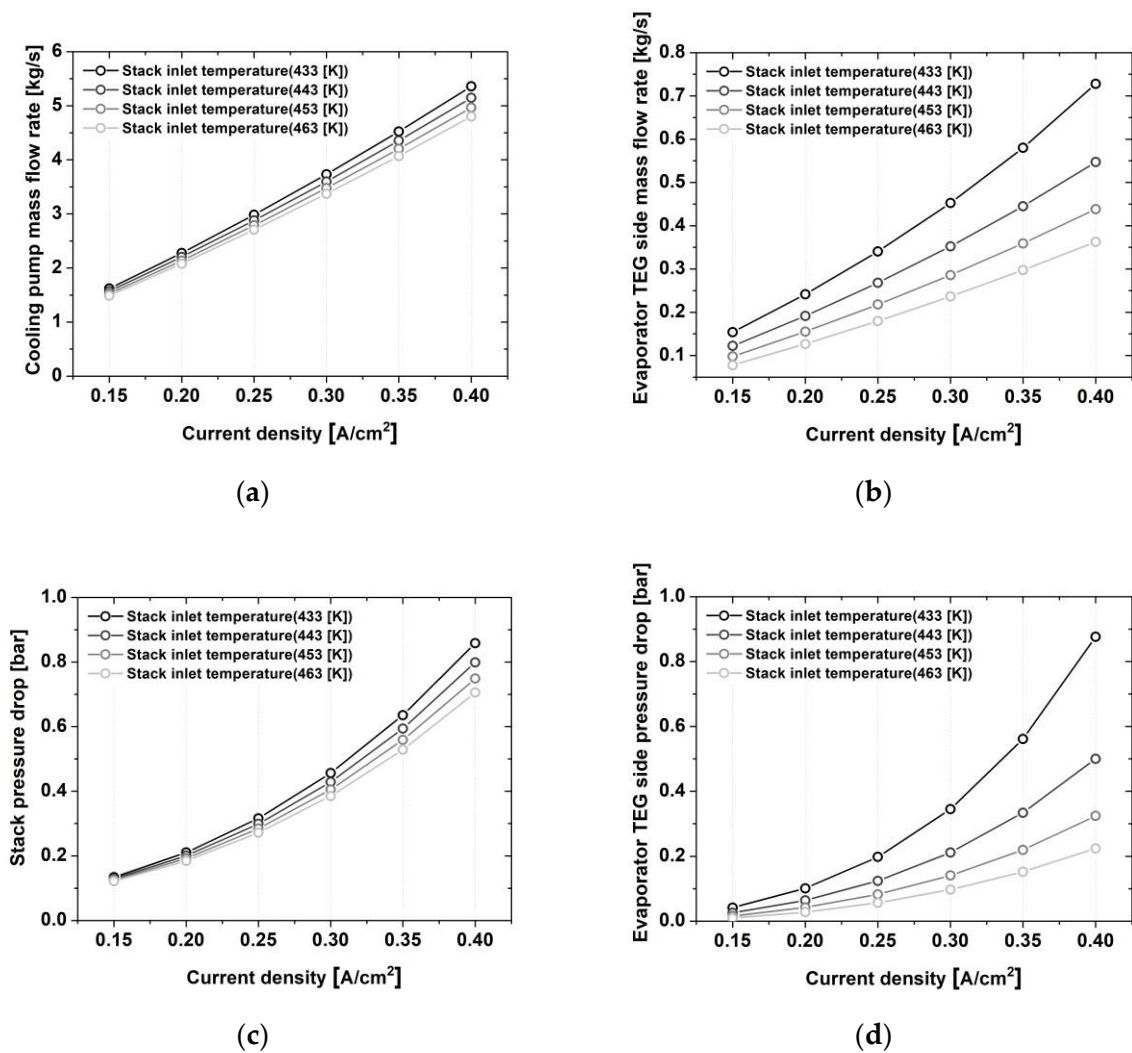


Figure 8. Validation trends of system loss and mass flow rate with stack inlet temperature. (a) Cooling pump mass flow rate; (b) Evaporator TEG side mass flow rate; (c) Stack pressure drop; (d) Evaporator TEG side pressure drop.

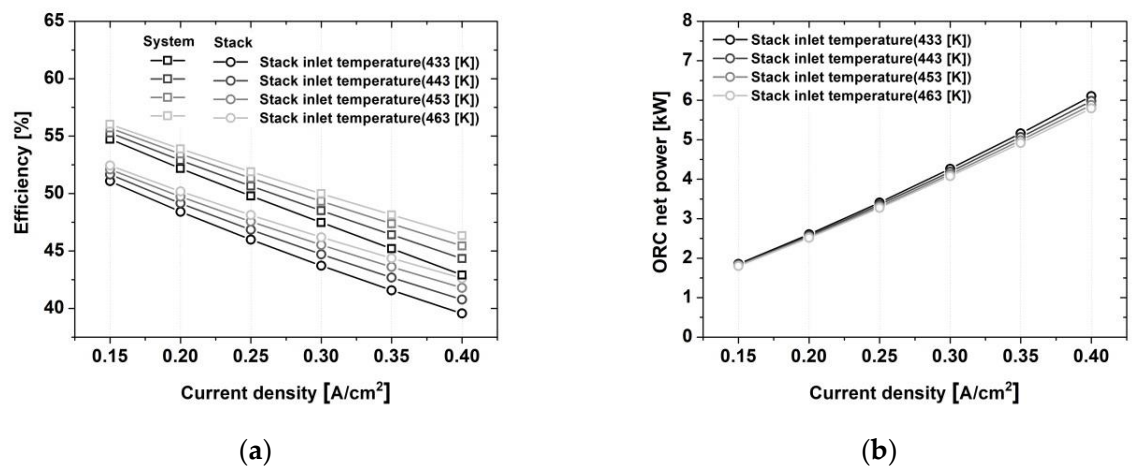


Figure 9. Cont.

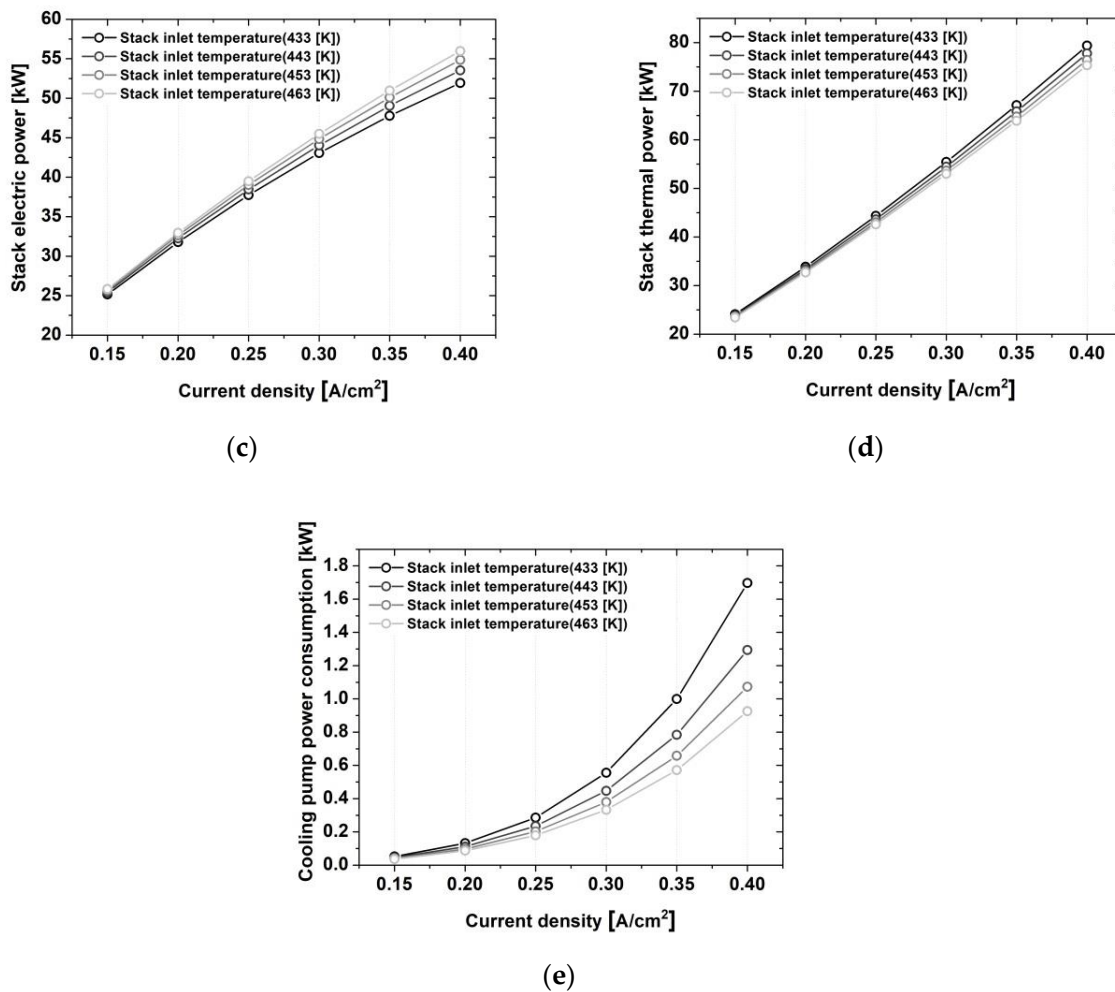


Figure 9. Validation trends of system performance with stack inlet temperature. (a) Combined system and stack power efficiency; (b) ORC net power; (c) Stack electric power; (d) Stack thermal power; (e) Cooling pump power consumption.

The efficiency of the combined system and the stack power efficiency are shown in Figure 9a, and the highest efficiency was shown as 56.03% and 52.45% at a current density of 0.15 A/cm² and a stack inlet temperature of 463 K. Additionally, the percentage increase in the combined system power efficiency compared to the stack power efficiency increased by up to 3.81% at a current density of 0.25 A/cm² and a stack inlet temperature of 433 K. In the case of the ORC net power, as the current density increased, the thermal power of the stack and the heat exchange amount of the evaporator increased, resulting in an increase in power generation. However, when the inlet temperature of the stack increased, the power generation decreased, and up to 0.3 kW decreased at a current density of 0.4 A/cm². In terms of the stack electric power, it reached a maximum of 55.96 kW at a current density of 0.4 A/cm² and 79.36 kW and a stack inlet temperature of 463 K as shown in Figure 9c, whereas in terms of the stack thermal power, it reached a maximum of 79.36 kW at a current density of 0.4 A/cm² and a stack inlet temperature of 433 K as shown in Figure 9d. As the current density increased, the power consumption of the cooling pump increased the required mass flow rate on the stack and the TEG side of the evaporator as shown in Figure 8, resulting in the increase in the corresponding pressure drop. As shown in Figure 9e, the power consumption of the cooling pump required a maximum of 1.69 kW at a current density of 0.4 A/cm² and a stack inlet temperature of 433 K.

Figure 10a shows the rate of change in the stack power, waste heat generation, and ORC power generation performance according to the difference of the stack coolant inlet temperature for each stack current density. As the current density is relatively higher, the rate of change in the stack power and

waste heat generation amount according to difference of the stack inlet temperature clearly increases. Additionally, the rate of change in power generation of stack considering power consumption of cooling pump is increased by up to 20% at current density of $0.4 \text{ A}\cdot\text{cm}^{-2}$ compared to rate of change in power considering only the stack model. On the other hand, the rate of change in the stack power, heat generation, and ORC power generation performance according to the current density for each inlet temperature showed a relatively low difference as shown in Figure 10b. Based on these system analysis results, the stack inlet temperature of the HT-PEMFC power generation system is judged as an important operating condition that affects the power generation performance change characteristics. In addition, while the effect of the difference of the current density for each the stack inlet temperature is relatively constant, the effect of the difference of the stack inlet temperature is expected to increase as the current density increases. Additionally, when cooling actuators such as a water pump and loss factors are added, the effect of stack operating temperature is expected to increase. In the case of the ORC system, the rate of change in power generation performance according to the temperature and current density was relatively low in the operating temperature range of this stack model.

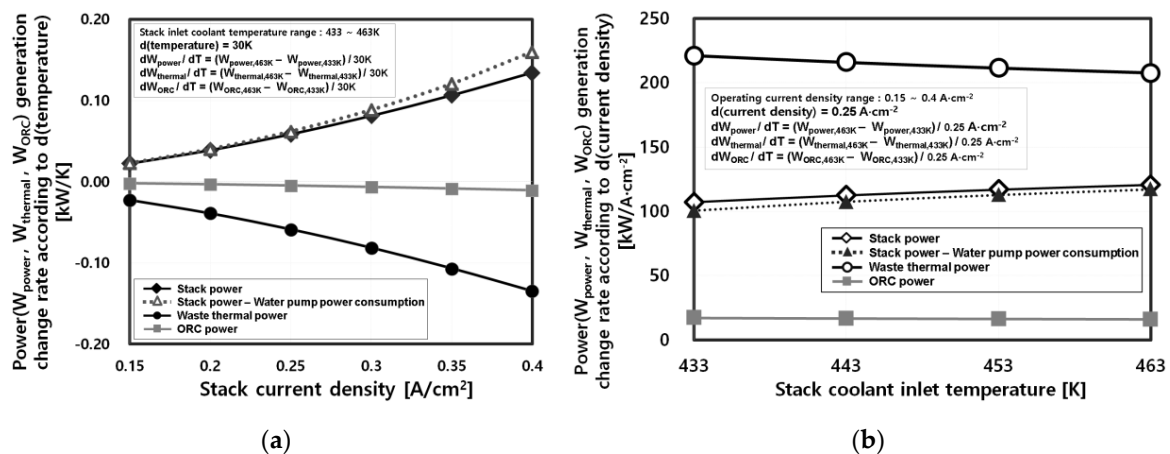


Figure 10. (a) The rate of change of stack power, waste heat generation, and ORC power generation according to operating temperature for each stack current density; (b) The rate of change in stack power, heat generation, and ORC power generation performance according to the current density for each stack coolant inlet temperature.

As shown in Figure 11, the system efficiency was compared excluding the stack power efficiency as a result of the coolant inlet temperature of the stack and condensing temperature of the working fluid formed at the condenser outlet for the ORC system. This is shown by excluding only the stack power generation from the overall efficiency of the combined power generation system. Through this, the efficiency changes of the ORC power generation system by pumps and heat exchangers excluding the stack were compared, and within the current density range, overall system efficiency except the stack tended to increase as the working fluid condensing temperature decreased. When the working fluid condensing temperature was $20 \text{ }^\circ\text{C}$, the maximum efficiency was about 4.75%, which was a 25% increase compared to the case where the working fluid condensing temperature was $35 \text{ }^\circ\text{C}$. Additionally, as the operating temperature of the stack increased, the deviation of the system efficiency except the stack tended to decrease relatively according to the change in current density. When the current density was $0.4 \text{ A}/\text{cm}^2$, the change in the system efficiency except the stack appeared to be the biggest according to the change of the stack operation temperature. This is believed to indicate that the influence of the operating temperature gradually increases under the power generation condition with the stack high load.

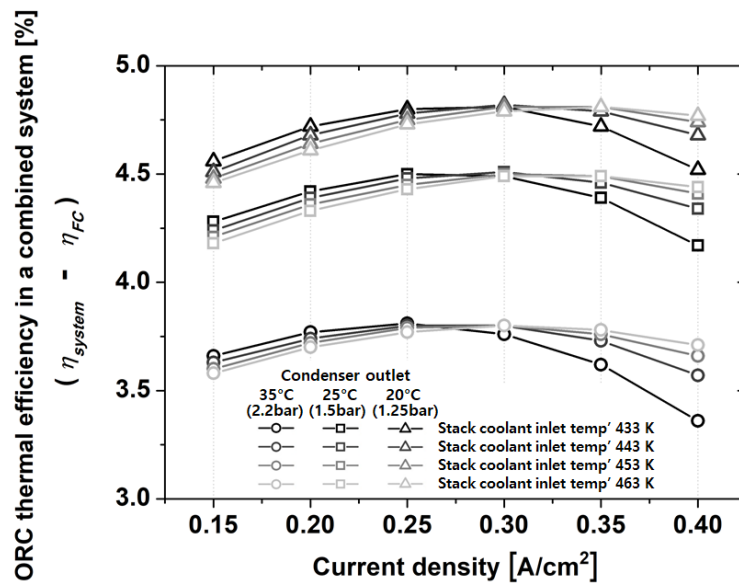


Figure 11. Difference between system and stack power efficiency with stack inlet temperature and condensing temperature.

5. Conclusions

In the case of HT-PEMFC, thermal management is formed as important as a relatively high operating temperature, and in the case of a heat exchange system that utilizes waste heat, since the operating range and strategies taking account of the thermal management of the stack must be selected, it is necessary to predict the power generation performance and efficiency according to the operating conditions. In this study, a model for a combined power generation system composed of a HT-PEMFC stack and an ORC power generation system was established, and the power generation performance and system efficiency were analytically compared according to the stack and ORC operating conditions. Each system was made of a model using the existing research contents and in the case of the plate heat exchanger for the Evaporator of the ORC system, which is the most important element for stack thermal management and waste heat recovery, reliability was secured by comparing the experimental results and the analysis results of the model. Through the analysis using the final combined power generation system model, the system power generation performance and efficiency were compared and predicted according to the operating temperature of the stack, the power generation load, and the ORC system working fluid condensing temperature, and the results are summarized as follows.

- (1) For the analytical comparative study, modeling of each of the HT-PEMFC stack and ORC combined power generation system was conducted. In particular, in order to secure the reliability of the plate heat exchanger for the ORC power generation system, previous experimental results under the same operating conditions and the model-based analysis results established in this study were compared. The reliability of the combined power generation system model was secured through this process.
- (2) Using the established combined power generation system model, the power generation performance and system efficiency of each stack and ORC system according to the power generation load and operating temperature of the HT-PEMFC stack were compared analytically. It is believed that the model has a higher degree utilization in a HT-PEMFC stack in which the higher the operating temperature within the allowable range, the higher the power generation and efficiency is. It also has higher degree utilization at a stack operating temperature where the waste heat that is proportional to the power generation load is relatively high. Furthermore, it is determined that the stack capacity and rated power generation section (current density range during power generation) need to be selected considering the target subjects as the amount

of waste heat becomes greater than the amount of power generated at points above a certain current density.

- (3) And as the current density is relatively higher, the rate of change in the stack power and waste heat generation amount according to the stack operating temperature clearly increases. Additionally, the rate of change in power generation by operating temperature of stack with cooling pump is increased by up to 20% at the current density of $0.4 \text{ A}\cdot\text{cm}^{-2}$ compared to rate of change in power considering only stack model. Therefore, the operating temperature of the HT-PEMFC stack generation system is able to be considered as an important operating condition that affects the power generation performance change characteristics.
- (4) In the model of the HT-PEMFC stack and ORC combined power generation system, comparative analysis was performed according to the operating temperature, power generation load (current density), and working fluid condensing temperature of the ORC system in order to compare the system efficiency excluding the stack, that is, the thermal efficiency of the ORC and subsystem that includes the stack cooling pump and heat exchanger, which change according to the operating conditions. As the operating temperature of the stack increased, the efficiency deviation of ORC and subsystem excluding the stack by the change in current density tended to decrease. Considering the energy load consumed by the thermal management part, it was shown that, under a certain current density, the lower the stack operation temperature was, and the more the efficiency of the ORC and subsystem except the stack improved. Moreover, as the working fluid condensing temperature decreased, the efficiency of the combined power generation system except for the stack tended to increase as well.

The HT-PEMFC stack and ORC combined power generation system require an appropriate operation strategy according to the target subjects and operating environment. To this end, this study constructed a combined power generation system model that considered the thermal management of the stack and the heat exchange process of waste heat and verified the operation range according to operating. It is believed that the results of this study will contribute to the selection of stacks and establishment of the strategies according to the target subjects and operation environments of the HT-PEMFC stack and ORC combined power generation system. In the future, an improvement on the model will be made regarding the target subjects of specific combined power generation, and analytical and experimental comparative studies will be conducted.

Author Contributions: H.S.K. designed the research, H.S.K., M.-H.K. and Y.H.S. discussed the results and contributed to writing the paper. All authors have read and agreed to the published version of the manuscript.

Funding: This research was supported by the Technology Development Program to Solve Climate Changes of the National Research Foundation (NRF) funded by the Ministry of Science, ICT & Future Planning (NRF-2016M1A2A2937158).

Conflicts of Interest: The authors declare no conflict of interest.

References

1. Arpino, F.; Massarotti, N.; Mauro, A.; Vanoli, L. Metrological analysis of the measurement system for a micro-cogenerative SOFC module. *Int. J. Hydrogen Energy* **2011**, *36*, 10228–10234. [[CrossRef](#)]
2. Arpino, F.; Dell'Isola, M.; Maugeri, D.; Massarotti, N.; Mauro, A. A new model for the analysis of operating conditions of micro-cogenerative SOFC unit. *Int. J. Hydrogen Energy* **2013**, *38*, 336–344. [[CrossRef](#)]
3. Duhn, J.D.; Jensen, A.D.; Wedel, S.; Wix, C. Optimization of a new flow design for solid oxide cells using computational fluid dynamics modelling. *J. Power Sources* **2016**, *336*, 261–271. [[CrossRef](#)]
4. Supra, J.; Janßen, H.; Lehnert, W.; Stolten, D. Temperature distribution in a liquid-cooled HT-PEFC stack. *Int. J. Hydrogen Energy* **2013**, *38*, 1943–1951. [[CrossRef](#)]
5. Lüke, L.; Janßen, H.; Kvesić, M.; Lehnert, W.; Stolten, D. Performance analysis of HT-PEFC stacks. *Int. J. Hydrogen Energy* **2012**, *37*, 9171–9181. [[CrossRef](#)]
6. Kandidayeni, M.; Macias, A.; Boulon, L.; Trovão, J.P.F. Online Modeling of a Fuel Cell System for an Energy Management Strategy Design. *Energies* **2020**, *13*, 3713. [[CrossRef](#)]

7. Dudek, M.; Raźniak, A.; Rosół, M.; Siwek, T.; Dudek, P. Design, Development, and Performance of a 10 kW Polymer Exchange Membrane Fuel Cell Stack as Part of a Hybrid Power Source Designed to Supply a Motor Glider. *Energies* **2020**, *13*, 4393. [[CrossRef](#)]
8. Jannelli, E.; Minutillo, M.; Perna, A. Analyzing microcogeneration systems based on LT-PEMFC and HT-PEMFC by energy balances. *Appl. Energy* **2013**, *108*, 82–91. [[CrossRef](#)]
9. Chen, X.; Li, W.; Gong, G.; Wan, Z.; Tu, Z. Parametric analysis and optimization of PEMFC system for maximum power and efficiency using MOEA/D. *Appl. Therm. Eng.* **2017**, *121*, 400–409. [[CrossRef](#)]
10. Bargal, M.H.; Abdelkareem, M.A.; Tao, Q.; Li, J.; Shi, J.; Wang, Y. Liquid cooling techniques in proton exchange membrane fuel cell stacks: A detailed survey. *Alex. Eng. J.* **2020**, *59*, 635–655. [[CrossRef](#)]
11. Najafi, B.; Mamaghani, A.H.; Rinaldi, F.; Casalegno, A. Long-term performance analysis of an HT-PEM fuel cell based micro-CHP system: Operational strategies. *Appl. Energy* **2015**, *147*, 582–592. [[CrossRef](#)]
12. Cardona, E.; Piacentino, A. A methodology for sizing a trigeneration plant in Mediterranean areas. *Appl. Therm. Eng.* **2003**, *23*, 1665–1680. [[CrossRef](#)]
13. Ziher, D.; Poredos, A. Economics of a trigeneration system in a hospital. *Appl. Therm. Eng.* **2006**, *26*, 680–687. [[CrossRef](#)]
14. He, T.; Shi, R.; Peng, J.; Zhuge, W.; Zhang, Y. Waste heat recovery of a PEMFC system by using organic rankine cycle. *Energies* **2016**, *9*, 267. [[CrossRef](#)]
15. Dickes, R.; Dumont, O.; Lemort, V. Experimental assessment of the fluid charge distribution in an organic Rankine cycle (ORC) power system. *Appl. Therm. Eng.* **2020**, *179*, 115689. [[CrossRef](#)]
16. Jang, Y.; Lee, J. Comprehensive assessment of the impact of operating parameters on sub 1-kW compact ORC performance. *Energy Convers. Manag.* **2019**, *182*, 369–382. [[CrossRef](#)]
17. Jeong, H.; Oh, J.; Lee, H. Experimental investigation of performance of plate heat exchanger as organic Rankine cycle evaporator. *Int. J. Heat Mass Transf.* **2020**, *159*, 120158. [[CrossRef](#)]
18. Yang, S.C.; Hung, T.C.; Feng, Y.Q.; Wu, C.J.; Wong, K.W.; Huang, K.C. Experimental investigation on a 3 kW organic Rankine cycle for low-grade waste heat under different operation parameters. *Appl. Therm. Eng.* **2017**, *113*, 756–764. [[CrossRef](#)]
19. Rosli, R.E.; Sulong, A.B.; Daud, W.R.W.; Zulkifley, M.A.; Husaini, T.; Rosli, M.I.; Majlan, E.H.; Haque, M.A. A review of high-temperature proton exchange membrane fuel cell (HT-PEMFC) system. *Int. J. Hydrogen Energy* **2017**, *42*, 9293–9314. [[CrossRef](#)]
20. Korsgaard, A.R.; Refshauge, R.; Nielsen, M.P.; Bang, M.; Kær, S.K. Experimental characterization and modeling of commercial polybenzimidazole-based MEA performance. *J. Power Sources* **2006**, *162*, 239–245. [[CrossRef](#)]
21. Korsgaard, A.R.; Nielsen, M.P.; Kær, S.K. Part one: A novel model of HTPEM-based micro-combined heat and power fuel cell system. *Int. J. Hydrogen Energy* **2008**, *33*, 1909–1920. [[CrossRef](#)]
22. Kang, H.S.; Shin, Y.H. Analytical Study of Tri-Generation System Integrated with Thermal Management Using HT-PEMFC Stack. *Energies* **2019**, *12*, 3145. [[CrossRef](#)]
23. Pukrushpan, J.T. Modeling and control of fuel cell systems and fuel processors. Ph.D. Thesis, University of Michigan, Ann Arbor, MI, USA, 2003.
24. Chang, H.; Wan, Z.; Zheng, Y.; Chen, X.; Shu, S.; Tu, Z.; Chan, S.H.; Chen, R.; Wang, X. Energy- and exergy-based working fluid selection and performance analysis of a high-temperature PEMFC-based micro combined cooling heating and power system. *Appl. Energy* **2017**, *204*, 446–458. [[CrossRef](#)]
25. Lee, H.S.; Lee, M.Y.; Cho, C.W. Analytic study on thermal management operating conditions of balance of 100 kW fuel cell power plant for a fuel cell electric vehicle. *J. Korea Acad. Ind. Coop. Soc.* **2019**, *16*, 1–6.
26. Muley, A.; Manglik, R.M. Experimental study of turbulent flow heat transfer and pressure drop in a plate heat exchanger with chevron plates. *J. Heat Transf.* **1999**, *121*, 110–117. [[CrossRef](#)]
27. Yan, Y.Y.; Lin, T.F. Evaporation Heat Transfer and Pressure Drop of Refrigerant R-134a in a Plate Heat Exchanger. *J. Heat Transf.* **1999**, *121*, 118–127. [[CrossRef](#)]

Publisher’s Note: MDPI stays neutral with regard to jurisdictional claims in published maps and institutional affiliations.



© 2020 by the authors. Licensee MDPI, Basel, Switzerland. This article is an open access article distributed under the terms and conditions of the Creative Commons Attribution (CC BY) license (<http://creativecommons.org/licenses/by/4.0/>).